2024 European Control Conference (ECC)
June 25-28, 2024. Stockholm, Sweden

Gain-scheduled Design of Active Braking Control Systems for Optimized Ground Handling in Aircraft

José Joaquín MENDOZA LOPETEGUI[1], Giulio FINOTTO[1], and Mara TANELLI[1]

Abstract— **Aircraft anti-skid systems are key to maintaining directional control during ground handling and must balance performance and robustness over a wide operational envelope. In particular, the impact of longitudinal speed on the braking dynamics induces an important coupling between the longitudinal and vertical dynamics due to the aerodynamic effects. In this paper, longitudinal slip-based and wheel speed deceleration-based anti-skid controllers are designed based on control-oriented models of the braking dynamics for an aircraft with a tricycle landing gear configuration. A gain-scheduling strategy is devised to achieve high performance and maintain stability during landing maneuvers. The stability of the resulting closed-loop system affected by parametric variability and discretization effects is later verified in the framework of Linear Parameter-Varying systems by formulating a set of efficient Linear Matrix Inequalities. The resulting anti-skid designs are successfully evaluated in a validated multibody simulator for a target aircraft.**

I. INTRODUCTION

Anti-skid systems in aircraft are fundamental to safety and efficiency during landing and rejected take-off maneuvers. On the one hand, they ensure that – upon brake pedal application by the pilot – the wheels do not go into a locked condition, thus causing severe ground handling issues and excessive wear on the tires. On the other hand, these systems seek to maximize braking performance and reduce braking distances along the runway by maximizing the exploitation of the available tire-runway friction. The two objectives are complementary to each other, which leads to a challenging design problem that requires the anti-skid system engineer to balance the aggressiveness of the controller with its robustness properties. Moreover, there is a wide variation range of parameters encountered in the operational envelope of the system, which have important effects on the dynamics of aircraft landings and rejected take-offs. Variables such as the runway friction condition, the aircraft inertial characteristics, or the dynamic variability of braking dynamics with respect to aircraft speed have to be considered.

The variability of the braking dynamics concerning longitudinal velocity is well-known in automotive anti-skid systems, and controller adaptation with respect to its variation is used to increase performance due to a dedicated tuning that captures the change in the open-loop response characteristics [1]. The phenomenon is even more pronounced in aircraft, as the braking maneuvers' speed induces significant load variations due to speed-dependent aerodynamic effects, yielding a coupling between the vertical and longitudinal dynamics.

The most common approach to designing aircraft anti-skid systems is based exclusively on the wheel deceleration measurement [2], [3], as no aircraft velocity knowledge is required, thus allowing the Brake Control Unit to work as an isolated system. In recent years, some attempts have been made to introduce more performing controllers based on the longitudinal wheel slip, see e.g., [4]–[7], mimicking techniques more widespread in the automotive realm [8]. The present work is a new attempt in this direction, and the main contributions are threefold. First, we propose gain-scheduled strategies akin to the ones found in advanced automotive systems to design both slip-based and deceleration-based aircraft anti-skid systems that are able to cope with the impact of longitudinal velocity on the braking system dynamics. Second, we provide a sound verification process based on formulating the closed-loop system dynamics as a Linear Parameter-Varying (LPV) System and checking the feasibility of appropriate Linear Matrix Inequality (LMI) conditions. Third, we compare the performance of the proposed methods on a validated aircraft simulator based on the metrics proposed by the SAE AIR1739B standard, commonly used in industry to evaluate aircraft anti-skid algorithms.

The structure of the paper is as follows. Section II describes the control problem and the simulation environment for its evaluation. Section III describes the control-oriented modeling, the structure of the anti-skid controllers, and the proposed gain-scheduling strategy. Section IV describes the approach used to verify the closed-loop stability of the designs under parametric variability as well as under controller discretization. Section V compares the performances of the two anti-skid designs on a set of braking maneuvers. Finally, Section VI provides some closing remarks.

II. PROBLEM DESCRIPTION AND SIMULATION ENVIRONMENT

This work is concerned with the design, verification, and performance evaluation of two aircraft anti-skid algorithms during a landing maneuver for a target aircraft for which experimental data was available, and that will serve as a case study. The aircraft under study has a landing gear in a tricycle configuration with only the Main Landing Gear (MLG) wheels equipped with a hydraulic braking system. It is assumed that the aircraft has established a proper ground contact by the moment the pilot presses the brake pedals, and also that the aircraft traces a straight trajectory along the runway so that the lateral dynamics can be neglected.

A model-based design of both a slip-based and a deceleration-based anti-skid controller will be conducted that satisfy a set of specifications in the form of minimum gain

[1]J. J. Mendoza Lopetegui, G. Finotto, and M. Tanelli are with the Dipartimento di Elettronica, Informazione e Bioingegneria, Politecnico di Milano, 20133 Milan, Italy (e-mail: josejoaquin.mendoza@polimi.it; giulio.finotto@mail.polimi.it; mara.tanelli@polimi.it).

Fig. 1. Isometric view of the multibody model in the Matlab/Simulink interface.

margins, phase margins, and bandwidth for different regions of the operational envelope. In particular, the system dynamics' strong dependence on the aircraft's longitudinal velocity calls for gain-scheduling strategies to achieve the performance objectives. Therefore, the proposed controller should also guarantee that the closed-loop stability is preserved when the controller's parameters are actively modulated.

A validated multibody simulator will be used to evaluate the algorithms' performance. The simulator runs in a Matlab/Simulink environment employing the Simscape Multibody library to describe the landing gear kinematics and dynamics of the target aircraft. In Fig. 1, a view of the aircraft is shown. The simulation environment includes a wide range of complex phenomena that have been modeled using experimental data from real landing maneuvers. The interested reader is referred to the work [9] for an in-depth description of the model's characteristics and a comparison between simulated and experimental data. For the purposes of this work, a brief overview of some relevant characteristics of the simulator follows. As seen in Fig. 1, the aircraft is modeled as a chain of rigid bodies connected by different sets of joints. The geometric and kinematic description of the landing gear retains the most important elements and constraints from the target aircraft. Detailed modeling has been employed to capture the shock absorber dynamics, the compliance that exists between the landing gear structural elements, and the track variation, which allows to mimic load transfer effects during a landing maneuver.

The contact between the runway and tire has been implemented using a Fiala model [10], with the appropriate parameters of the tires being extracted from the supplier's data. The longitudinal friction coefficient μ is described by a Burckhardt model [11], with the following relationship:

$$\mu(\lambda) = \theta_1 \left(1 - e^{-\lambda\theta_2}\right) - \lambda\theta_3 \tag{1}$$

with θ_1, θ_2 and θ_3 the parameters that describe the runway condition, and λ is the longitudinal wheel slip. This work uses eight friction conditions to evaluate the anti-skid algorithms' robustness to environmental variability. In Fig. 2, a graphical representation of the friction curves is shown. Also relevant for anti-skid design is the braking actuator model. The simulation environment describes the generation of braking torque T_b at the disc brakes of the MLG from an input pressure command P_b^{ref} given by the anti-skid controller. The model is shown in Fig. 3. More precisely, the model illustrated in Fig. 3 assumes that a low-level high-bandwidth closed-loop pressure controller is in place that tracks a given reference pressure command

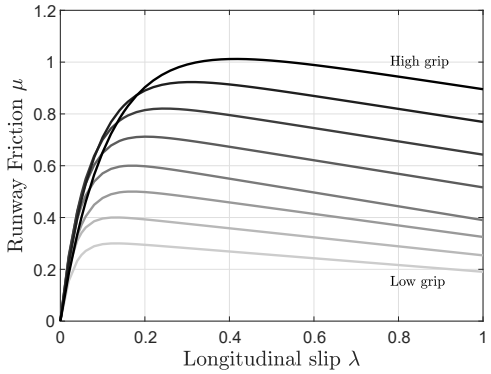

Fig. 2. Burckhardt friction model. The eight represented curves allow conditions ranging from wet/slippery surfaces (bottom curves) to dry/high-grip surfaces (top curves).

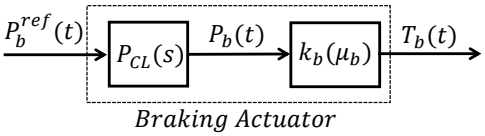

Fig. 3. Schematic representation of the braking actuator dynamics.

P_b^{ref}, as is common in industrial practice. The low-level pressure controller can be represented as a second-order transfer function $P_{CL}(s)$, with a cutoff frequency of around 20 Hz. In turn, the pressure P_b at the end of the hydraulic line is converted to an effective braking torque T_b through the conversion coefficient k_b, which depends on the braking friction coefficient μ_b between the wheel brake assembly and the disc brakes. See [12] for details on the modeling of the braking actuator. Finally, a set of external forces affect the aircraft during a landing maneuver. In particular, a drag force $F_D = C_{drag} v_a^2$ is applied opposite to the direction of movement of the aircraft, described by a conventional quadratic dependence on the longitudinal velocity v_a with a drag coefficient C_{drag}; a residual thrust force F_{th} is applied along the direction of movement using a nonlinear map depending on the aircraft velocity v_a; and a lift force $F_L = C_{lift} v_a^2$ is applied in the vertical direction, also described by a quadratic dependence on v_a with a lift coefficient C_{lift}.

III. CONTROLLER DESIGN

In this Section, the two anti-skid controllers are designed. For each one, a control-oriented model is developed based on a simplified representation of the dynamics. Then, the controller structure is presented, as well as the tuning strategy adopted to cope with the design constraints. Note that in each design, an independent anti-skid controller operates on each MLG side having the same parameters, so that both MLG anti-skid controllers are symmetric. For this reason, the design of a single MLG side will be described. The general scheme valid for both designs is shown in Fig. 4.

A. Slip-based Controller

The slip-based controller aims to control the value of the longitudinal wheel slip λ, defined as:

$$\lambda = (v_a - \omega r)/v_a, \tag{2}$$

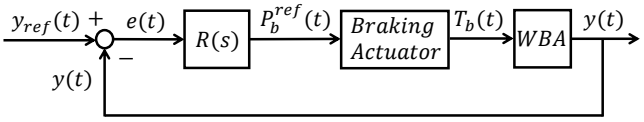

Fig. 4. General anti-skid control design scheme. WBA stands for Wheel Brake Assembly.

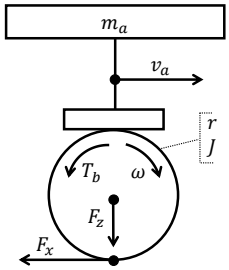

Fig. 5. Single corner model of the braking dynamics.

where ω is the rotational wheel speed, v_a is the longitudinal aircraft speed, and r is the effective radius of the wheel. Referring to Fig. 4, $y(t) = \lambda(t)$ in this case.

1) Control-oriented Model: A simple yet effective model of the slip dynamics is the single corner model, used both in automotive [8] and aerospace [3] realms to capture the most important dynamical effects at the wheel level. A representation of the model is shown in Fig. 5, where m_a is the load sustained by a single MLG side, J is the wheel inertia, while F_z and F_x are the vertical and longitudinal forces at the contact patch, respectively. The implicit assumptions involve neglecting the vertical suspension dynamics, the tire compression, and the load transfer effect along the pitch axis. Considering that the time constants of the rotational dynamics of ω and the longitudinal dynamics of v_a are vastly different, it can be assumed that v_a is a slowly-varying parameter $\overline{v}_a$ from the point of view of the braking dynamics, which evolve according to the relationship:

$$J\dot{\omega} = rF_x - T_b \tag{3}$$

By combining the definition of λ in (2), Eq. (3), the static conversion between pressure and torque in the braking actuator, and assuming a linear relationship between the vertical and longitudinal forces of the form $F_x = F_z\mu(\lambda)$, the slip dynamics are obtained:

$$\dot{\lambda} = -\frac{1}{\overline{v}_a}\Big(\frac{1-\lambda}{m_a} + \frac{r^2}{J}\Big)F_z\mu(\lambda) + \frac{r}{J\overline{v}_a}k_b(\mu_b)P_b \tag{4}$$

Finally, by linearizing Eq. (4) around an equilibrium ($\overline{\lambda}$,$\overline{P}_b$) the following transfer function can be obtained:

$$G^{\lambda}_{P_b}(s) = \frac{\frac{k_b(\overline{\mu}_b)r}{J\overline{v}_a}}{s + \frac{F_z\mu_1(\overline{\lambda})}{\overline{m}_a\overline{v}_a}\Big[\Big((1-\overline{\lambda}) + \frac{\overline{m}_a r^2}{J}\Big)\Big]} \tag{5}$$

where $\overline{\mu}_b$ is the average friction coefficient value, $\overline{m}_a$ is the average single corner mass over the operational envelope, and where it has been assumed that $\mu_1(\overline{\lambda})$ is significantly larger than $\mu(\overline{\lambda})$ with $\mu_1(\overline{\lambda})$ the slope of the friction curve at the equilibrium. The anti-skid system can enforce the assumption with an appropriate choice of the reference $\overline{\lambda}$.

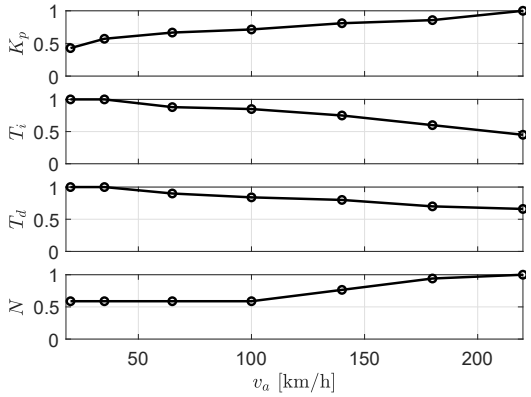

Fig. 6. Normalized gain-scheduling laws for $R_\lambda(s)$.

2) Controller Tuning and Scheduling Strategy: Equation (5) includes parameters that depend implicitly on the aircraft velocity v_a, as both the wheel radius r and the effective vertical force F_z are affected by the lift force F_{lift}. Therefore, the resulting transfer function is highly affected by v_a, which makes it an immediate candidate for a gain-scheduling strategy. Referring to Fig. 4, the structure of the proposed controller $R(s) = R_\lambda(s)$ in its continuous-time version is a Proportional-Integral-Derivative (PID) controller:

$$R_\lambda(s) = K_p(v_a)\left(1 + \frac{1}{T_I(v_a)s} + \frac{T_D(v_a)s}{\frac{T_D(v_a)}{N(v_a)}s + 1}\right) \tag{6}$$

where the free variables have been scheduled in v_a. The controller implementation includes a conventional anti-windup back-calculation strategy to handle the integral term. To tune the parameters, the longitudinal velocity range has been partitioned into seven regions, ranging from 18 km/h to 220 km/h, with a higher granularity towards the low-speed regime since the open loop braking dynamics get infinitely fast at low speeds [1]. For each region, a controller $R^i_\lambda(s)$ with $i = \{1, ..., 7\}$ is tuned on the loop function $L^i_\lambda(s) = R^i_\lambda(s)P_{CL}(s)G^{\lambda}_{P_b}(s)$ to achieve a phase margin $\phi_m \geq 75°$ and gain margin $g_m \geq 20$ dB for all speeds v_a in its corresponding region. Moreover, the imposed crossover frequency ω_c on each $L^i_\lambda(s)$ is progressively reduced at lower speeds to account for the open loop braking dynamics variability. The tuning for each velocity region is shown in the appropriate columns in Table I. Note a small overlap was introduced in the first two regions to handle the low-speed regime smoothly. The parameters for $R^i_\lambda(s)$ are assigned to the centroid of its corresponding region. Each tuning parameter then is linearly interpolated in v_a to construct the gain-scheduling lookup table, shown in Fig. 6, which is expressed in normalized units for confidentiality reasons.

B. Deceleration-based Controller

The deceleration-based controller aims to control the value of the normalized wheel deceleration η, defined as:

$$\eta = -(\dot{\omega}r)/g, \tag{7}$$

with g the gravitational acceleration. In Fig. 4, $y(t) = \eta(t)$. The dynamics of η are the basis for the controller design.

TABLE I

PHASE MARGIN ϕ_m, GAIN MARGIN g_m AND CROSSOVER FREQUENCY ω_c OF $L^i_{\lambda/\eta}(s)$ FOR EACH REGION i ON BOTH ANTI-SKID DESIGNS

Velocity		**λ-based**		**η-based**	
Region [km/h]	$\omega_c[Hz]$	$\phi_m[^\circ]$	$g_m[dB]$	$\phi_m[^\circ]$	$g_m[dB]$
$18 \leq v_a \leq 30$	1	130	20	110	20
$20 \leq v_a \leq 50$	1.5	130	20	110	20
$50 \leq v_a \leq 80$	1.5	120	20	100	20
$80 \leq v_a \leq 120$	2	110	25	90	25
$120 \leq v_a \leq 160$	2.5	105	25	90	25
$160 \leq v_a \leq 200$	2.5	85	25	90	20
$200 \leq v_a \leq 220$	2.5	75	30	75	20

1) Control-oriented Model: The single corner model illustrated in Fig. 5 is also used to design this controller. In this case, combining Eqs. (3) and (7) we obtain:

$$\eta = r(T_b - rF_z\mu(\lambda))/(Jg) \tag{8}$$

Similarly as done in Section III-A.1, by linearizing Eq. (8) around an equilibrium ($\overline{\eta}$,$\overline{P}_b$), using the static conversion between pressure and torque, assuming a linear relationship between the vertical and longitudinal forces, and assuming that $\mu_1(\overline{\lambda})$ is significantly larger than $\mu(\overline{\lambda})$, we obtain:

$$G^{\eta}_{P_b}(s) = \frac{k_b(\overline{\mu}_b)r}{Jg} \frac{s + \frac{F_z}{\overline{m}_a \overline{v}_a}[(1-\overline{\lambda})\mu_1(\overline{\lambda})]}{s + \left[\frac{F_z}{\overline{v}_a}\left(\left(\frac{1-\overline{\lambda}}{m_a} + \frac{r^2}{J}\right)\mu_1(\overline{\lambda})\right)\right]} \tag{9}$$

2) Controller Tuning and Scheduling Strategy: Equation (9) is also highly affected by the longitudinal velocity v_a, for which a similar scheduling strategy as the one designed in III-A.2 will be proposed. Referring to Fig. 4, the structure of the proposed controller $R(s) = R_\eta(s)$ in its continuous-time version consists of two poles and one zero to achieve a loop function of the same relative degree as in III-A.2:

$$R_\eta(s) = K(v_a)\frac{s+a_1(v_a)}{s(s+b_1(v_a))} = \frac{A(v_a)}{s} + \frac{B(v_a)}{s+b_1(v_a)} \tag{10}$$

where $A(v_a) = K(v_a)a_1(v_a)/b_1(v_a)$, $B(v_a) = K(v_a)(b_1(v_a) - a_1(v_a))/b_1(v_a)$, while K, a_1, and b_1 are the parameters of the controller. Note that the last expression in Eq. (10) isolates the purely integral term, which is also handled with an anti-windup back-calculation strategy. The same scheduling strategy in v_a as the one in III-A.2 is used. The same seven velocity regions are used, and for each one, a controller $R^i_\eta(s)$ is tuned on the loop function $L^i_\eta(s) = R^i_\eta(s)P_{CL}(s)G^\eta_{P_b}(s)$ to achieve a phase margin $\phi_m \geq 75^\circ$ and gain margin $g_m \geq 20$ dB for all speeds v_a in its region. The tuning for each velocity region is shown in the appropriate columns in Table I. The obtained gain-scheduling lookup table is shown in Fig. 7.

Remark 1: The design of both controllers is complemented by an adaptive reference that seeks the friction curve's peak by a heuristic typical of industrial algorithms. However, its description is left out due to space limitations.

Remark 2: Note that for the scope of this work, the velocity v_a is assumed to be known. A practical implementation requires some estimation strategy. For the η-based controller, since v_a is only used in the scheduling phase, a simple algorithm as the one in [13] can be used. In the λ-based case, a more involved methodology is needed, as in [14].

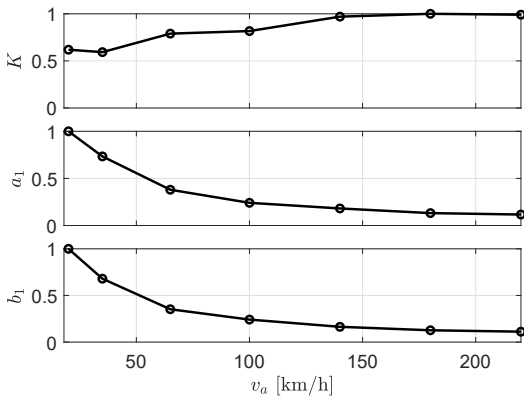

Fig. 7. Normalized gain-scheduling laws for $R_\eta(s)$.

IV. CONTROLLER VERIFICATION

In this Section, the verification of the stability properties of both anti-skid designs is conducted. First, the stability of the closed-loop system is checked against the parametric variations induced by the operational envelope of the system by appropriate Linear Matrix Inequality (LMI) conditions. Then, the stability is also checked against the discretization process to obtain the implementable controller $R_{\lambda/\eta}(z)$.

A. LPV Problem Formulation

Once the loop function $L_{\lambda/\eta}(s) = R_{\lambda/\eta}P_{CL}(s)G^{\lambda/\eta}_{P_b}(s)$ is operated in closed loop, a Linear Parameter-Varying (LPV) system is obtained. In particular, the velocity v_a continuously decreases during a braking maneuver, which has important effects on the dynamics, as analyzed in Section III. Moreover, the dynamics depend on the instantaneous friction exploited out of the runway, represented by $\mu_1(\lambda)$. Therefore, an uncertainty parameter vector $p = [v_a, \mu_1(\lambda)]$ is defined. Vector $p = p(t)$ is an unknown function of time, and the values it assumes define the parameter space $\mathbb{P}$. To verify the stability of the closed-loop system inside $\mathbb{P}$, a state space representation of the system dependent on $p \in \mathbb{P}$ is obtained:

$$\begin{aligned} \dot{x}(t) &= A(p)x(t) + B(p)\overline{u}(t) \\ \overline{y}(t) &= C(p)x(t) \end{aligned} \tag{11}$$

where $\overline{u}(t) = \lambda_{ref}(t)$ or $\eta_{ref}(t)$ while $\overline{y}(t) = \lambda(t)$ or $\eta(t)$, depending on each controller design. For numerical conditioning reasons, the transformation between the closed-loop transfer functions and system (11) for every value of p has been obtained using a balanced realization.

B. LMI Feasibility Conditions

The stability of system (11) can be assessed by resorting to a useful result shown in [15], originally developed in [16]:

Theorem 1: The closed-loop system (11) is stable if there exists a C^1 matrix function $X(p)$ satisfying:

$$X(p) > 0 \tag{12}$$

$$A^T(p)X(p) + X(p)A(p) + \sum_{j=1}^{M} \pm \nu_j \frac{\partial X(p)}{\partial p_j} < 0 \tag{13}$$

with $M = 2$ the dimensionality of the parameter space $\mathbb{P}$, ν_j an element of vector ν that satisfies $|\dot{p}(t)| \leq \nu$ element-wise, and the operator $\pm$ indicates that every combination of signs should be taken into account in the second inequality so that Eq. (13) represents 2^M inequalities. The bounds ν_j can be obtained by physical considerations. In particular, ν_1 corresponds to the magnitude of the maximum aircraft longitudinal deceleration, which can be computed by noting that $m_a \dot{v}_a = -F_x$ so that $|\dot{v}_a|$ is maximized at the peak of the friction curve in a high-grip condition during the low-speed regime in which the effective load F_z is maximum. An additional slack can be included in the bound ν_1 to account for the drag force F_D. In turn, ν_2 is related to the maximum rate of change of the runway friction conditions. More concretely, $\dot{\mu}_1 = (\partial \mu_1 / \partial \lambda)\dot{\lambda}$ where the first factor can be computed by Eq. (1) while the second one is shown in Eq. (4) in which all terms are bounded as long as $\overline{v}_a > 0$.

The conditions shown in Theorem 1 can be formulated as a finite-dimensional problem by a gridding approach [15]. First, a basis for the matrix function $X(p)$ is chosen to set a dependence on p. Then, the parameter space $\mathbb{P}$ is gridded so that for each point in the grid, the conditions from Eqs. (12) and (13) can be numerically checked. For both anti-skid designs, the following linear basis has been employed:

$$X(p = [v_a \;\; \mu_1]) = X_0 + X_1 v_a + X_2 \mu_1 \tag{14}$$

The chosen basis allows to cast efficiently the problem as an LMI with X_0, X_1, and X_2 as unknowns. Parameter v_a has been divided into 202 grid points equally spaced ranging from 18 km/h to 220 km/h. Instead, eight grid points have been selected for the parameter μ_1, each one corresponding to the slope of each friction curve $\mu(\lambda)$ evaluated at $\overline{\lambda} = 0.12$, which is a value located at the stable part of all the curves, compatible with a high-performing anti-skid system. Hence, the gridding of $\mathbb{P}$ is constituted by 1616 points. The previous approach leads to a system of 6465 LMIs for each anti-skid design. The conditions were checked via YALMIP [17] and SeDuMi [18], which verifies the closed-loop system stability under the gain-scheduling approach.

C. Discretization Verification

Both anti-skid controllers $R_{\lambda/\eta}(s)$ are discretized by a Tustin discretization scheme with a sampling time of T_s = 1 ms to obtain $R_{\lambda/\eta}(z)$. To verify that the stability properties of the resulting LPV system are not lost during the discretization, the approach from [19] is considered. The following expression indicates the upper bound T_d that preserves the stability of the closed-loop system:

$$T_d = \max_{p \in \mathbb{P}} \left(\max_{\lambda \in \sigma(A(p)) \text{ and } Im(\lambda)=0} \frac{2}{Re(\lambda)} \right) \tag{15}$$

where $\sigma(A)$ indicates the spectrum of matrix A. Using the same gridding strategy as the one from Section IV-B, it has been verified that for both controllers, $T_s < T_d$ and thus the discretization process preserves stability.

V. PERFORMANCE EVALUATION

In this Section, the controllers are evaluated in a set of braking maneuvers using the simulator from Section II. The maneuvers and the performance metrics used are described. Then, a summary of the results obtained is shown.

TABLE II
EVALUATED LANDING CONFIGURATIONS

CONFIGURATION	**Mass** [kg]	**Initial Speed** v_0 [km/h]
Light landing	2800	180
Medium landing 1	3150	195
Medium landing 2	3300	190
Heavy landing	4450	220

A. Simulated Scenarios and Performance Indexes

A braking maneuver is simulated by initializing the aircraft with a set of inertial parameters and initial velocity v_0. Four conditions relevant to the case study are considered and shown in Table II. The four conditions are combined with the eight friction curves from Fig. 2 for a total of 32 scenarios. For each case, a virtual pilot fully presses the pedals simultaneously on both MLG sides and requests maximum braking pressure within 1 second. The anti-skid system will actively regulate the pressure, aiming to maximize braking performance until the end of the maneuver at 18 km/h, in which the anti-skid disengages. Three performance indexes compliant with SAE AIR1739B [20] are used for evaluation:

- **Braking Distance (BD)**: Runway length travelled from braking maneuver start until anti-skid disengagement.
- **Developed μ efficiency (J_μ)**: Indicates how well the anti-skid system can exploit the runway friction condition. For each MLG wheel, it is defined as:

$$J_\mu = \Big(\int_{t_{start}}^{t_{end}} \mu(t) dS(t) \Big) / \Big(\int_{t_{start}}^{t_{end}} \mu_{max}(t) dS(t) \Big) \tag{16}$$

  with t_{start} and t_{end} the starting and ending times of the maneuver, $dS(t)$ the infinitesimal space displacement, while $\mu(t)$ and $\mu_{max}(t)$ are the exploited friction and the maximum attainable one at time t, respectively. The average for both MLG wheels is considered.
- **Stopping Distance Efficiency** (η_{dist}): Ratio of the perfect braking distance by always braking at the peak of the friction curve over the actual braking distance.

B. Results

The results for the two designs over the operational envelope are shown in Table III. Across all maneuvers, no wheel locking events were observed, indicating that the gain-scheduling approach was effective while actively modulating the controller parameters. From Table III, it can be noted that the slip-based controller significantly outperformed the deceleration-based one, in line with what has been observed in automotive braking dynamics [8]. As a representative example, in Fig. 8 a maneuver using the slip-based controller for a configuration of 3300 kg of mass and high grip runway is shown. As can be seen, the anti-skid controller maintains a value close to the peak of the friction curve for most of the maneuver. In contrast, in Fig. 9, the same braking maneuver is conducted with the deceleration-based algorithm, which is markedly slower to get close to the optimal friction value but nonetheless maintains the system stability.

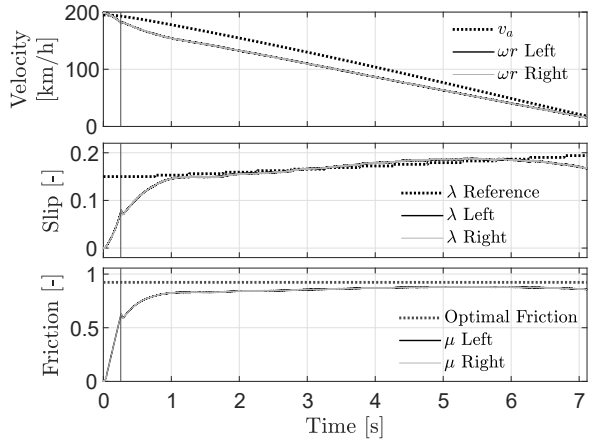

Fig. 8. Braking maneuver with aircraft mass of 3300 kg, high grip, and slip-based anti-skid. Top plot: Longitudinal aircraft velocity and wheel speeds. Middle plot: Longitudinal slip and corresponding reference. Bottom plot: Effectively exploited friction and optimal friction.The vertical line indicates the anti-skid system engagement.

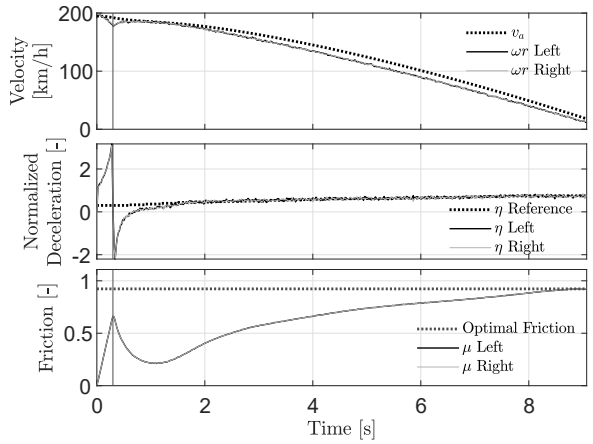

Fig. 9. Braking maneuver with aircraft mass of 3300 kg, high grip, and deceleration-based anti-skid. Top plot: Longitudinal aircraft velocity and wheel speeds. Middle plot: Normalized wheel deceleration and corresponding reference. Bottom plot: Effectively exploited friction and optimal friction. The vertical line indicates the anti-skid system engagement.

VI. CONCLUDING REMARKS

This paper studied the problem of designing robust and performing aircraft anti-skid algorithms for a tricycle landing gear configuration. A model-based control design process was illustrated that incorporated a velocity-based gain-scheduling law that adapts the parameters of the controllers during a braking maneuver to maximize performance. Moreover, the stability of the resulting closed-loop systems was studied in the framework of Linear Parameter-Varying systems and later checked in simulation using a validated multibody model of the target aircraft. As future research directions, ongoing efforts are being devoted to conducting a practical implementation of the slip-based controller, as well as to integrating the slip-based controller in a ground handling system for pilot assistance during landings.

TABLE III

AVERAGE VALUE OF THE PERFORMANCE INDEXES

Anti-skid Controller	BD **[m]**	J_μ **[%]**	η_{dist} **[%]**
λ-based anti-skid	480.21	96.24	92.99
η-based anti-skid	541.23	71.55	69.79

REFERENCES

[1] T. A. Johansen, I. Petersen, J. Kalkkuhl, and J. Ludemann, "Gain-scheduled wheel slip control in automotive brake systems," *IEEE Transactions on Control Systems Technology*, vol. 11, no. 6, pp. 799–811, 2003.

[2] L. D'Avico, M. Tanelli, S. Savaresi, M. Airoldi, and G. Rapicano, "A deceleration-based algorithm for anti-skid control of aircraft," *IFAC-PapersOnLine*, vol. 50, no. 1, pp. 14 168–14 173, 2017, 20th IFAC World Congress.

[3] Z. Jiao, Z. Wang, D. Sun, X. Liu, Y. Shang, and S. Wu, "A novel aircraft anti-skid brake control method based on runway maximum friction tracking algorithm," *Aerospace Science and Technology*, vol. 110, p. 106482, 2021.

[4] M. Q. Chen, W. S. Liu, Y. Z. Ma, J. Wang, F. R. Xu, and Y. J. Wang, "Mixed slip-deceleration PID control of aircraft wheel braking system," *IFAC PapersOnLine*, vol. 51, no. 4, pp. 160–165, 2018.

[5] M. Chen, F. Xu, X. Liang, and W. Liu, "MSD-based NMPC aircraft anti-skid brake control method considering runway variation," *IEEE Access*, vol. 9, pp. 51 793–51 804, 2021.

[6] N. Bai, X. Liu, J. Li, Z. Wang, P. Qi, Y. Shang, and Z. Jiao, "An aircraft brake control algorithm with torque compensation based on RBF neural network," *Chinese Journal of Aeronautics*, vol. 37, no. 1, pp. 438–450, 2024.

[7] A. W. Ndiaye, J.-M. Biannic, M. Cassaro, C. Combier, and J.-B. Lestage, "Advanced Aircraft Braking Control Laws Design and Validation," in *9th European Conference for Aeronautics and Space Sciences (EUCASS)*, 2021, pp. 1–16.

[8] S. Savaresi and M. Tanelli, *Active Braking Control Systems Design for Vehicles*. London, UK: Springer-Verlag, 2010, ISBN 978-1-84996-350-3.

[9] J. J. Mendoza Lopetegui, G. Papa, M. Morandini, and M. Tanelli, "Shock absorber leakage impact on aircraft lateral stability during ground handling maneuvers," *Journal of Guidance, Control, and Dynamics*, vol. 46, no. 6, pp. 1066–1082, 2023.

[10] E. Fiala, "Seitenkraften am rollenden luftreifen (Lateral forces on rolling pneumatic tires)," *Zeitschrift des Vereines Deutscher Ingenieure (V.D.I.) (Journal of the Association of German Engineers)*, vol. 96, no. 29, pp. 973–979, 1954.

[11] M. Burckhardt, *Fahrwerktechnik: Radschlupf-Regelsysteme (Chassis technology: Wheel slip control systems)*. Wüzburg, Germany: Vogel Verlag, 1993, ISBN 978-3-80-230477-4.

[12] J. J. Mendoza Lopetegui, G. Papa, M. Morandini, and M. Tanelli, "Data-driven modeling and regulation of aircraft brakes degradation via antiskid controllers," *IEEE Transactions on Reliability*, vol. 72, no. 3, pp. 889–899, 2023.

[13] Z. Ming, N. Hong, W. Xiao-hui, and Z. Enzhi, "Research on modelling and simulation for aircraft anti-skid braking," in *2008 2nd International Symposium on Systems and Control in Aerospace and Astronautics*, 2008, pp. 1–5.

[14] G. Papa, M. Tanelli, G. Panzani, and S. M. Savaresi, "Wheel-slip estimation for advanced braking controllers in aircraft: Model based vs. black-box approaches," *Control Engineering Practice*, vol. 117, p. 104950, 2021.

[15] M. Corno, M. Tanelli, S. M. Savaresi, and L. Fabbri, "Design and validation of a gain-scheduled controller for the electronic throttle body in ride-by-wire racing motorcycles," *IEEE Transactions on Control Systems Technology*, vol. 19, no. 1, pp. 18–30, 2010.

[16] F. Wu, X. H. Yang, A. Packard, and G. Becker, "Induced L2-norm control for LPV systems with bounded parameter variation rates," *International Journal of Robust and Nonlinear Control*, vol. 6, no. 9-10, pp. 983–998, 1996.

[17] J. Lofberg, "Yalmip: A toolbox for modeling and optimization in matlab," in *2004 IEEE International Conference on Robotics and Automation*, 2004, pp. 284–289.

[18] J. F. Sturm, "Using sedumi 1.02, a MATLAB toolbox for optimization over symmetric cones," *Optimization Methods and Software*, vol. 11, no. 1-4, pp. 625–653, 1999.

[19] R. Tóth, F. Felici, P. Heuberger, and P. Van den Hof, "Crucial aspects of zero-order hold LPV state-space system discretization," *IFAC Proceedings Volumes*, vol. 41, no. 2, pp. 4952–4957, 2008.

[20] SAE Wheels, Brakes and Skid Controls Committee, "Information on antiskid systems," *SAE Aerospace, Standard AIR1739B*, 2016.